

Influence of Respiratory Gating, Image Filtering, and Animal Positioning on High-Resolution Electrocardiography-Gated Murine Cardiac Single-Photon Emission Computed Tomography

Chao Wu, Pieter E.B. Vaissier, Brendan Vastenhouw, Johan R. de Jong, Riemer H.J.A. Slart, and Freek J. Beekman

Abstract

Cardiac parameters obtained from single-photon emission computed tomographic (SPECT) images can be affected by respiratory motion, image filtering, and animal positioning. We investigated the influence of these factors on ultra-high-resolution murine myocardial perfusion SPECT. Five mice were injected with 99m technetium (^{99m}Tc)-tetrofosmin, and each was scanned in supine and prone positions in a U-SPECT-II scanner with respiratory and electrocardiographic (ECG) gating. ECG-gated SPECT images were created without applying respiratory motion correction or with two different respiratory motion correction strategies. The images were filtered with a range of three-dimensional gaussian kernels, after which end-diastolic volumes (EDVs), end-systolic volumes (ESVs), and left ventricular ejection fractions were calculated. No significant differences in the measured cardiac parameters were detected when any strategy to reduce or correct for respiratory motion was applied, whereas big differences ($> 5\%$) in EDV and ESV were found with regard to different positioning of animals. A linear relationship ($p < .001$) was found between the EDV or ESV and the kernel size of the gaussian filter. In short, respiratory gating did not significantly affect the cardiac parameters of mice obtained with ultra-high-resolution SPECT, whereas the position of the animals and the image filters should be the same in a comparative study with multiple scans to avoid systematic differences in measured cardiac parameters.

IN ADDITION TO tissue properties of the myocardium such as perfusion or viability, electrocardiography (ECG)-gated cardiac single-photon emission computed tomography (SPECT) can provide quantitative information about ventricular volumes, ventricular ejection fractions, and myocardial wall motion and thickness.^{1–4} In such studies, image quality can degrade due to respiratory motion. Respiratory gating has been applied in tomography studies too, for example, for imaging lung areas.^{5,6} It involves

rebinning of the projection data into respiratory gates that represent different breathing phases. As the position and orientation of the heart are also affected by respiratory motion, it is prudent to investigate whether respiratory gating may also reduce image blur in cardiac imaging and improve cardiac imaging quality. As early as 1998, the scheme for simultaneous ECG and respiratory gating (“dual gating”) and an algorithm for respiratory motion compensation were already developed and tested with phantoms for clinical positron emission tomography (PET).⁷ It was found that the magnitude of the motion induced by respiration is close to the myocardial wall thickness.^{8,9} As a result of this study, many clinical cardiac studies are performed with simultaneous ECG and respiratory gating to obtain better resolved myocardial walls in the reconstructed images.^{10,11}

ECG gating has been evaluated for small animal SPECT for assessing left ventricular function and has been applied in studies where new pharmaceuticals were tested.^{12–18} Simultaneous ECG and respiratory gating has been assessed for a high-resolution (1 mm) microPET system.¹⁹ In this study, it was found that although respiratory motion was detectable in the images, its spatial extent and duration were

From the Section Radiation, Detection & Medical Imaging, Delft University of Technology, Delft, the Netherlands; Rudolf Magnus Institute of Neuroscience, University Medical Center Utrecht, Utrecht, the Netherlands; MILabs B.V., Utrecht, the Netherlands; and Department of Nuclear Medicine and Molecular Imaging, University Medical Center Groningen, University of Groningen, Groningen, the Netherlands.

Address reprint requests to: Chao Wu, PhD, Section Radiation, Detection & Medical Imaging, Delft University of Technology, Building 50, Mekelweg 15, 2629 JB, Delft, the Netherlands; e-mail: c.wu@tudelft.nl.

DOI 10.2310/7290.2014.00052

© 2014 Decker Intellectual Properties

DECKER
X

small, and it could therefore likely be ignored for most studies. However, whether the assessment of cardiac function in SPECT with sub-half-millimeter resolution can benefit from simultaneous ECG and respiratory gating has not yet been investigated.

Image filtering is another factor that may influence the assessment of cardiac function. Cardiac quantification software usually fits a flexible three-dimensional (3D) model of the left ventricle to the reconstructed activity in the myocardium and calculates cardiac parameters via this model. Image filtering changes the smoothness and thickness of the reconstructed activity in the ventricular wall, which may result in changes in the fit of the 3D model to the left ventricle in the image. Therefore, image filtering may change cardiac parameters that are calculated from the fitted model. The effects of filtering have already been observed in many clinical studies.^{20–24} However, no investigations of filtering effects on murine cardiac SPECT have yet been published.

The position of an animal (supine or prone) during scanning affects arterial filling, which may result in differences in the cardiac parameters that are measured. This has already been investigated in clinical studies.^{25–27} In these studies, changes in the left ventricular volume were detected, but no significant differences in ejection fraction were found. However, such a study has yet to be performed for small animal cardiac SPECT. A change in animal position may also change restrictions on thoracic movement and thus may result in different levels of heart motion due to respiration.

The aim of the present study was to investigate the influence of respiratory gating, postreconstruction image filtering, and mouse positioning on high-resolution ECG-gated 99m technetium (^{99m}Tc)-tetrofosmin myocardial perfusion SPECT.

Materials and Methods

Animal studies were conducted following protocols approved by the Animal Research Committee of the University Medical Center Utrecht.

In Vivo Myocardial Perfusion SPECT of Mice

The U-SPECT-II (MILabs B.V., Utrecht, the Netherlands) multipinhole system was used in the present work. This dedicated small animal SPECT system has stationary detectors. The highest achievable spatial resolution of this system is < 0.4 mm for ^{99m}Tc imaging when using a general-purpose mouse collimator (as was used in the

present study and is recommended by the manufacturer) with 75 pinholes (0.6 mm diameter). The system accepts three transistor-transistor logic (TTL) trigger signals for gated studies through three Bayonet Neill-Concelman (BNC) connectors mounted on the side panel. Both trigger and photon-counting events are recorded in list mode.²⁸

Five C57-BL6/J mice (about 30 g each) were injected via the tail vein with 200 to 250 MBq ^{99m}Tc-tetrofosmin in 0.3 to 0.4 mL. For each mouse, two focused cardiac SPECT scans were performed, the first scan starting about 30 minutes postinjection. The first scan lasted 60 minutes, whereas the second scan lasted 70 minutes to obtain approximately equal numbers of counts in both scans (i.e., to compensate for the decay of ^{99m}Tc). For each mouse, one scan was performed with the mouse in a supine position, whereas the other scan was performed with the mouse in a prone position, and the position order was alternated for different mice to avoid bias caused by the order of positioning. A heating pad was placed between the mice and the animal bed. The mice were anesthetized with a mixture of 1.6 to 2.0% isoflurane in medical air (Univentor, UNO B.V., Zevenaar, the Netherlands). ECG signals were measured by using three ECG leads (Neonatal Monitoring Electrode, 3M, Maplewood, MN), and the respiratory signal was measured by using a respiration sensor (Graseby Respiration Sensor, Medicare, Kilmacanogue, Ireland). Both signals were sent to an animal monitoring and gating module (BioVet, m2m Imaging, Cleveland, OH). Two channels of trigger signals were produced by this device (one channel for ECG signals and one channel for respiratory signals), and these signals were sent to the U-SPECT-II system via two BNC connectors.

Image Reconstruction and Strategies for Respiratory Motion Compensation

Trigger events were recovered during list-mode data processing. A histogram of the time intervals between adjacent ECG trigger events was made for each scan, and a window was set to accept only the intervals in the main peak (width about 12%) of the histogram. This way, most irregular heartbeats and spurious or missing trigger signals were rejected. The same procedure was performed for the time intervals between adjacent respiratory trigger events. Next, each accepted ECG interval was divided into eight cardiac phases, and each accepted respiratory interval was split into eight respiratory phases. This resulted in 64 combinations of cardiac and respiratory phases. Each photon count in the list-mode data was sorted into one of 64 projection data sets depending on how its time stamp

located in the ECG and respiratory intervals, as illustrated in Figure 1.

Images were reconstructed by a pixel-based ordered subset expectation maximization algorithm (POSEM)²⁹ with 16 subsets, and 6 iterations were performed. The voxel size of the reconstructions was 0.2 mm. To study the influence of respiratory motion, three different strategies were applied to form 8 ECG-gated heart images from the 64 dual gated images.

First, for the “standard strategy,” images of all eight respiratory gates that were in the same cardiac phase were averaged directly. This way, the counts in all respiratory phases were used, and no respiratory motion correction was applied.

Second, for the “motion-reduced strategy,” images of the second up to the seventh respiratory gates that were in the same cardiac phase were averaged directly. This strategy is based on a hypothesis that significant respiratory motion occurs only when a respiratory trigger signal is created, which was revealed in Yang and colleagues.¹⁹ This way, counts acquired in respiratory gates that correspond to the largest

respiratory motions were excluded from image formation, and the resulting images may be less influenced by respiration.

Third, for the “motion-corrected strategy,” images of all eight respiratory gates that were in the same cardiac phase were first registered to each other and then averaged. Details of the registration procedure are discussed in the following section.

Image Registration for Respiratory Motion Correction

Contraction and relaxation of the heart (i.e., cardiac phases) mainly change the shape of the heart, whereas respiratory motion primarily changes the position and orientation of the heart as the diaphragm, the chest wall, and the lungs move during breathing.⁷ The influence of respiratory motion on the cardiac images can therefore be corrected by using a rigid registration procedure. In principle, any dual-gated image can serve as a reference image for the registration of dual gated images that correspond to the same cardiac phase but to different respiratory phases. However, the noise level in the 64 individual dual gated images was relatively high because of the relatively low number of counts with which each image was reconstructed. Therefore, we did not determine the registration parameters from these images directly; rather, we calculated these parameters from eight respiratory-only gated images: each of these images was an average of eight dual gated images that corresponded to one respiratory phase but to different cardiac phases. The resulting image corresponding to the fifth respiratory phase served as the reference image for registration of the images corresponding to the other respiratory phases. As a result, seven transformation matrices were obtained. These transformations were then applied to the 56 dual gated images that corresponded to the first to fourth and sixth to eighth respiratory phases.

The transformation matrices were calculated using the elastix toolbox.³⁰ The normalized correlation coefficient (NCC) between two images was selected as the metric for registration. To avoid influence of high activity uptake in the liver and the gallbladder on the registration procedure, a 3D elliptical mask that only covered the heart was used. This mask was fixed to the reference image, and the transformation matrices were calculated using only the voxels inside the mask region.

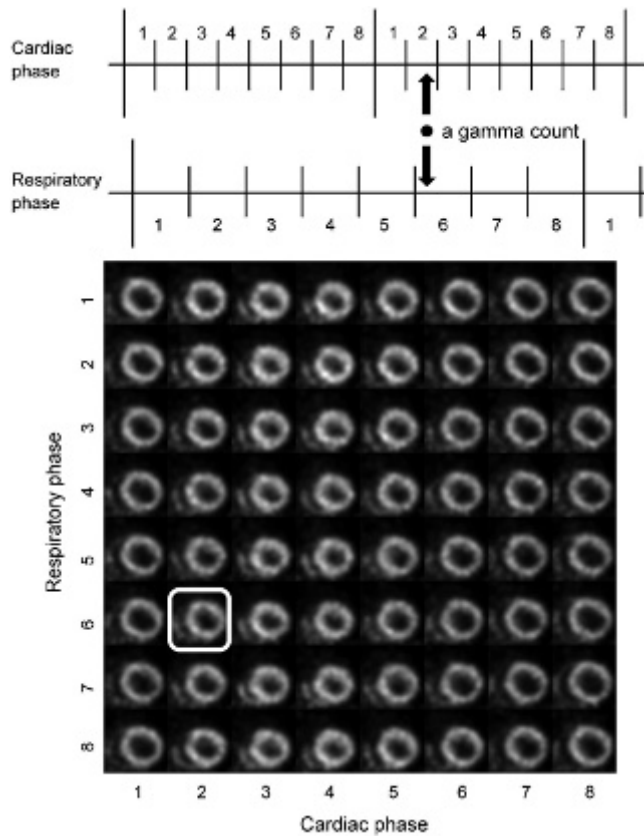


Figure 1. Dual gating scheme with eight ECG and eight respiratory gates. A count that is, for example, in the second cardiac phase and the sixth respiratory phase will be sorted into the projection data set corresponding to this combination of phases. The reconstructed image for this combination of phases is indicated by the white box.

Image Processing and Analysis

All ECG-gated images that were obtained by the three strategies (standard, motion reduced, and motion corrected)

were spatially filtered with gaussian kernels of 0.5, 0.6, 0.7, 0.8, 0.9, and 1.0 mm full width at half maximum (FWHM) and then filtered along temporal frames (cardiac phases) by means of a circular convolution with a (0.25, 0.5, 0.25) kernel function. We analyzed these images with *Corridor4DM* software (INVIA, Ann Arbor, MI).³¹ For the clinical *Corridor4DM* software to accept mouse heart images, the voxel size of the images was changed from 0.2 to 2 mm. The cardiac volumes that were calculated by the software were rescaled afterwards to correspond to the original voxel size.

After importing the images into *Corridor4DM*, an initial manual reorientation of each image was performed to roughly align the heart's short axis (SA), vertical long axis (VLA), and horizontal long axis (HLA) with the three cartesian axes, after which the software automatically fine-tuned the orientation using a built-in algorithm. Next, a flexible 3D left ventricle (LV) model was fitted to the LV walls in the images. The model uses gradient operators, contiguity assumptions, and weighted spline interpolators to detect and refine the LV endocardial and epicardial surfaces.³¹ Using this model, the left ventricular volume (LVV) in each cardiac phase was calculated and the maximum and minimum LVVs of all cardiac phases were, respectively, defined to be the end-diastolic volume (EDV) and end-systolic volume (ESV). The left ventricular ejection fraction (LVEF) was also provided by the software.

In addition to cardiac parameters, images were directly compared by generating line profiles along different positions and directions in the images. To this end, an extra rigid registration was applied between the images.

Results

Respiratory Motion and Image Profiles

The transformation matrices that were obtained with the motion-corrected strategy revealed that the largest heart motion (about 1 mm translation) occurred in the eighth respiratory phase in which the respiratory trigger signal was created. The second largest heart motion (about 0.4 mm) occurred in the first phase, whereas the heart motions in the rest of the respiratory phases were generally less than 0.2 mm (Figure 2A), which is smaller than the highest resolution that the imaging system can achieve (about 0.35 mm). This finding is consistent with the hardware-recorded respiratory signal (Figure 2B) and with the hypothesis that significant respiratory motion occurs only when a respiratory trigger signal is created, which is the justification for the motion-reduced strategy (i.e., only using the second up to the seventh respiratory gate).

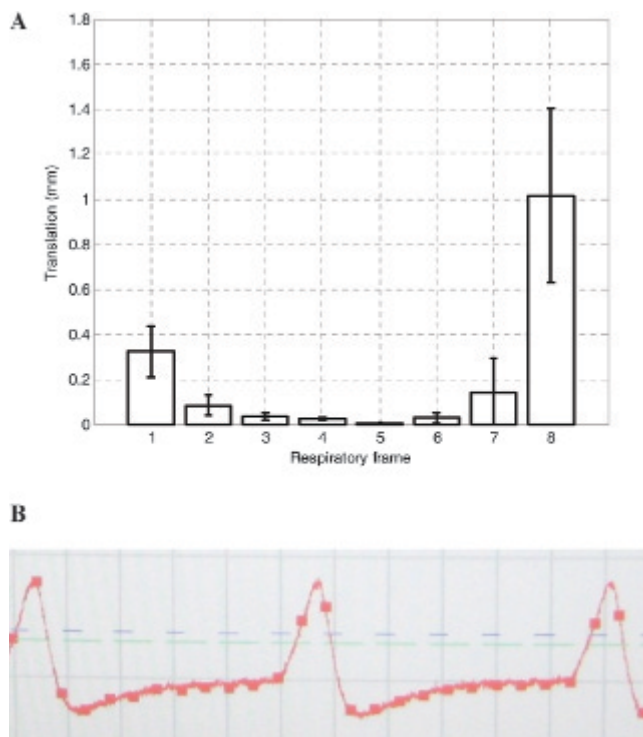


Figure 2. A, Respiratory heart translations that were calculated by the rigid registration procedure in the motion-corrected strategy. Relatively large translations were found only in the first and eighth frames on average over all scans. B, Signal recorded by respiration sensor.

Taking mouse 2 and mouse 5 as an example, almost no visual differences were found between the cardiac image slices and profiles corresponding to the three motion correction strategies (Figure 3).

Cardiac Parameters

The 180 ECG-gated heart images, resulting from all combinations between the five mice, the two positions, the three respiratory motion correction strategies, and the six gaussian filter kernels, were analyzed by *Corridor4DM* software. The resulting cardiac parameters are listed in Table 1. The EDV, ESV, and LVEF obtained from the images that were formed by the “standard strategy” and that were filtered with a 0.7 mm FWHM kernel were, respectively, $50 \pm 11 \mu\text{L}$, $22 \pm 8 \mu\text{L}$, and 0.57 ± 0.07 (average over the 10 scans). The mean values corresponding to this strategy and filter kernel served as reference values for comparing cardiac parameters obtained by other combinations of motion correction strategies and filter kernels. Note that in this work, the values of LVEF are expressed as decimal fractions to distinguish them from

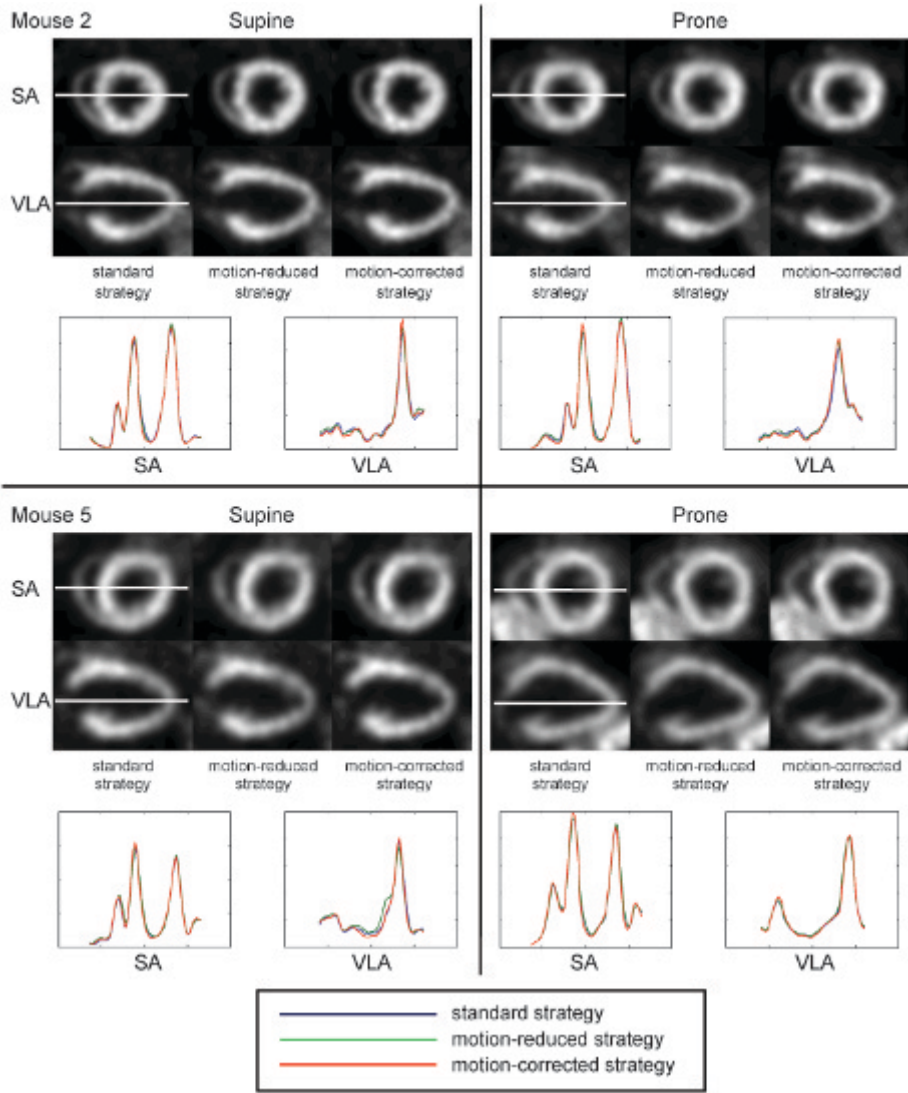


Figure 3. Short axis (SA) and vertical long axis (VLA) slices and line profiles of mouse 2 and mouse 5 in the supine and prone positions at end diastole. Images are filtered with a gaussian kernel (0.7 mm full width half maximum).

the relative changes in LVEF, which are expressed as percentages.

The 180 ECG-gated heart images were separated into 36 different groups, each group corresponding to a combination of one of the three motion correction strategies, one of the two animal positions, and one of the six filter kernels (each group contained reconstructions of five mouse scans). The average EDVs, ESVs, and LVEFs were calculated for each group. The results are plotted in Figure 4. This figure clearly shows that there were only slight changes in cardiac parameters induced by the different motion correction strategies. To investigate the effects of image filtering, animal positioning, and motion correction strategies on the measured cardiac parameters, we performed linear regression analyses on the 180 images (i.e., observations). The variables are listed in Table 2. The variable *prone* is a categorical dummy for animal

positioning, and *mr* and *mc* are categorical dummies for respiratory motion correction strategies. The supine position and the “standard strategy” were the reference categories in the regression. We also created categorical dummies *m2* to *m5* to represent individual differences between the mice. We omitted any interaction terms between the variable filter and the categorical dummies mentioned above because the effects of image filtering should have no correlation with possible effects induced by the other variables. Therefore, the dummies contributed only in the intercepts of the regression.

The linear regression model is represented by the following:

$$\begin{aligned} dep_i = & \beta_0 + \beta_1 filter_i + \beta_2 prone_i + \beta_3 mr_i + \beta_4 mc_i \\ & + \beta_5 m2_i + \beta_6 m3_i + \beta_7 m4_i + \beta_8 m5_i + \varepsilon_i \end{aligned} \quad (1)$$

Table 1. Cardiac Parameters Measured from Reconstructed Images

Filter (mm)	EDV (μL)						ESV (μL)						LVEF					
	Supine			Prone			Supine			Prone			Supine			Prone		
	S	MR	MC	S	MR	MC	S	MR	MC	S	MR	MC	S	MR	MC	S	MR	MC
Mouse 1 (31 g)																		
0.5	59	59	58	50	51	48	26	27	25	18	19	18	.56	.54	.58	.64	.62	.63
0.6	58	58	57	49	50	47	25	25	24	17	19	17	.56	.57	.58	.65	.63	.64
0.7	58	58	57	48	50	47	24	25	23	18	18	16	.59	.56	.59	.63	.64	.65
0.8	57	58	56	47	48	46	24	24	23	17	18	16	.57	.59	.59	.63	.62	.66
0.9	56	57	56	46	48	45	24	23	22	17	16	15	.57	.59	.60	.64	.66	.66
1.0	55	56	55	45	47	44	22	23	22	15	16	15	.59	.60	.60	.66	.65	.67
Mouse 2 (30 g)																		
0.5	40	39	39	40	40	39	16	17	16	19	19	18	.59	.57	.59	.51	.52	.54
0.6	39	39	39	39	39	38	16	16	15	18	19	17	.60	.58	.60	.54	.53	.55
0.7	39	39	38	39	39	38	16	16	15	17	19	17	.60	.59	.60	.56	.52	.56
0.8	38	38	38	39	38	37	14	16	14	16	17	16	.62	.59	.63	.58	.55	.57
0.9	38	38	37	38	37	37	13	15	13	15	17	16	.64	.61	.65	.60	.55	.58
1.0	37	37	37	37	36	36	13	13	13	15	16	15	.65	.64	.65	.59	.56	.58
Mouse 3 (30 g)																		
0.5	38	39	38	42	43	42	14	13	13	16	16	14	.62	.68	.66	.62	.62	.67
0.6	38	39	38	41	42	41	14	12	12	15	16	14	.64	.69	.68	.62	.62	.65
0.7	37	38	37	41	42	40	13	13	12	14	16	13	.66	.67	.68	.65	.63	.67
0.8	37	37	36	40	41	40	12	12	11	14	14	13	.68	.68	.68	.65	.65	.67
0.9	36	37	35	40	40	39	12	11	11	13	14	12	.67	.69	.69	.68	.65	.71
1.0	35	36	34	39	40	37	11	11	11	13	13	12	.69	.69	.69	.67	.68	.68
Mouse 4 (30 g)																		
0.5	58	61	56	65	65	65	24	27	24	31	31	31	.58	.56	.57	.53	.52	.53
0.6	58	61	56	64	65	65	25	26	23	31	31	31	.58	.57	.60	.51	.52	.53
0.7	58	59	56	64	64	64	24	26	22	30	31	31	.59	.56	.60	.53	.52	.52
0.8	55	59	54	63	64	63	23	24	22	30	30	31	.57	.59	.59	.52	.52	.51
0.9	54	56	52	63	63	63	23	23	21	30	30	30	.58	.58	.60	.53	.52	.52
1.0	53	56	52	62	62	63	22	23	21	28	29	29	.59	.59	.60	.55	.54	.53
Mouse 5 (31 g)																		
0.5	54	54	54	68	68	68	29	29	27	37	37	37	.46	.47	.51	.46	.45	.46
0.6	54	53	54	68	67	67	28	28	26	37	37	36	.48	.47	.51	.46	.45	.46
0.7	53	53	53	67	67	67	29	27	26	36	37	36	.46	.49	.50	.46	.45	.46
0.8	52	52	52	67	67	67	28	26	26	35	35	35	.47	.50	.50	.48	.47	.48
0.9	52	51	51	66	66	66	27	27	25	34	35	34	.49	.48	.51	.48	.48	.48
1.0	51	51	50	65	66	66	25	25	24	34	33	33	.52	.50	.52	.48	.50	.50

EDV = end-diastolic volume; ESV = end-systolic volume; LVEF = left ventricular ejection fraction; MC = motion-corrected strategy; MR = motion-reduced strategy; S = standard strategy.

in which i denotes the index of observations and dep represents the dependent variables (i.e., edv , esv , or $lvef$) in the three regressions. The estimates of the ordinary-least-squares (OLS) estimators (by *Stata*, StataCorp, College Station, TX) are listed in Table 3.

The coefficient of determination (R^2) of each regression was larger than 0.85, which means that the data points fit the regression model quite well. Before any causal interpretations of the results are made, the statistical significance of

the estimates at a 5% significance level is examined. Only if an estimated coefficient is statistically significant can one state that the effect of the corresponding parameter exists. In this study, we found strong evidence that filtering and animal positioning have an influence on EDV, ESV, and LVEF because the p values for the estimated coefficients for $filter$ ($\hat{\beta}_1$) and $prone$ ($\hat{\beta}_2$) were .00 ($< .05$) for all regressions. However, the p values for the estimated coefficients for mr ($\hat{\beta}_3$) and mc ($\hat{\beta}_4$) were all larger than .05, except for $\hat{\beta}_4$ in the

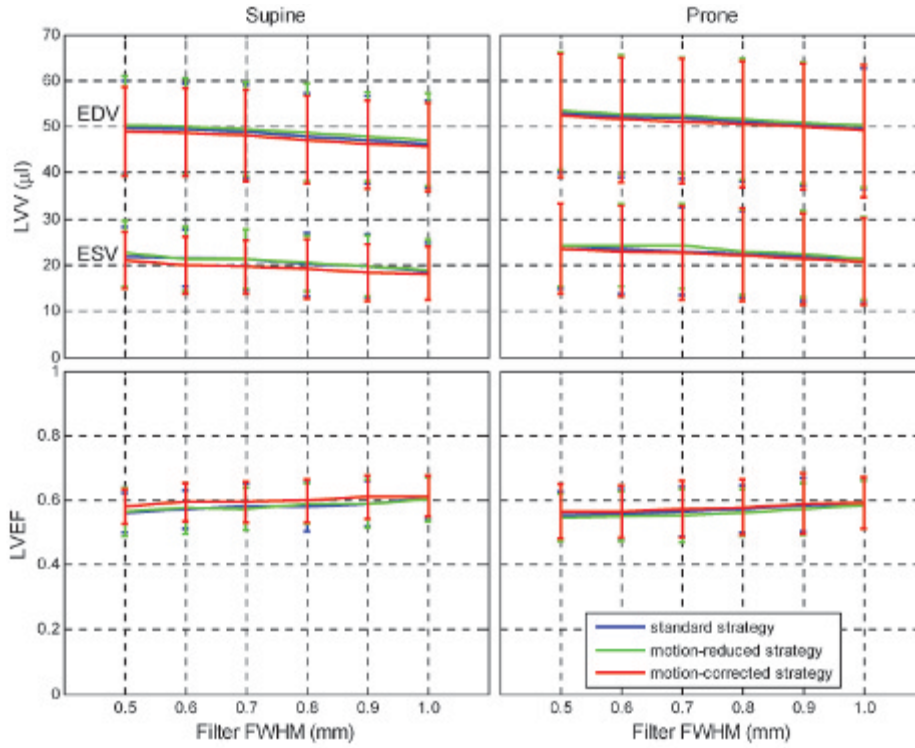


Figure 4. Effects of positioning, motion correction strategy, and gaussian filter size on left ventricular end-diastolic volumes (EDV), end-systolic volumes (ESV), and left ventricular ejection fractions (LVEFs) (average over all scans). LVV = left ventricular volume.

LVEF regression. Hence, we can conclude that compared to the “standard strategy,” the influence of the “motion-reduced” or “motion-corrected” strategies on the measured cardiac parameters are statistically insignificant at a 5% significance level; however, the “motion-corrected strategy” induced a statistically significant change to the LVEF. The changes in cardiac parameters for each of the significant OLS estimates are listed in Table 4.

We also noticed that the estimated parameters for dummies $m2$ to $m5$ are significant (their p values are $< .05$).

This means that the individual differences in the measured cardiac parameters were much bigger than the differences that could be induced by the different respiratory motion correction strategies.

Discussion

In this study, three respiratory motion correction strategies were examined to study the influence and potential benefit of respiratory motion compensating for ultra-high-resolution

Table 2. Description of Variables in Regression Analyses

Variable	Description
Dependent	
<i>edv</i>	End-diastolic volume (in μL)
<i>esv</i>	End-systolic volume (in μL)
<i>lvef</i>	Left ventricular ejection fraction (expressed as decimal)
Independent	
<i>filter</i>	FWHM (in mm) of gaussian filter
<i>prone</i>	Dummy variable (= 1 for prone position and = 0 for supine position)
<i>mr</i>	Dummy variable (= 1 for motion-reduced strategy and = 0 for others)
<i>mc</i>	Dummy variable (= 1 for motion-corrected strategy and = 0 for others)
<i>m2</i>	Dummy variable (= 1 for mouse 2 and = 0 for others)
<i>m3</i>	Dummy variable (= 1 for mouse 3 and = 0 for others)
<i>m4</i>	Dummy variable (= 1 for mouse 4 and = 0 for others)
<i>m5</i>	Dummy variable (= 1 for mouse 5 and = 0 for others)

FWHM = full width half maximum.

Table 3. OLS Estimates of Regression of EDV, ESV, and LVEF by Using a Linear Model

<i>Estimate</i>	<i>Mean</i>	<i>Standard Error</i>	<i>p Value</i>	<i>R</i> ²
EDV				
$\hat{\beta}_1$ (for <i>filter</i>)	−6.70	1.81	.000	0.8552
$\hat{\beta}_2$ (for <i>prone</i>)	3.13	0.62	.000	
$\hat{\beta}_3$ (for <i>mr</i>)	0.57	0.76	.456*	
$\hat{\beta}_4$ (for <i>mc</i>)	−0.65	0.76	.393*	
$\hat{\beta}_5$ (for <i>m2</i>)	−14.14	0.98	.000	
$\hat{\beta}_6$ (for <i>m3</i>)	−13.58	0.98	.000	
$\hat{\beta}_7$ (for <i>m4</i>)	7.69	0.98	.000	
$\hat{\beta}_8$ (for <i>m5</i>)	7.31	0.98	.000	
$\hat{\beta}_0$ (constant)	55.82	1.62	.000	
ESV				
$\hat{\beta}_1$ (for <i>filter</i>)	−6.14	1.25	.000	0.8608
$\hat{\beta}_2$ (for <i>prone</i>)	2.50	0.43	.000	
$\hat{\beta}_3$ (for <i>mr</i>)	0.42	0.52	.425*	
$\hat{\beta}_4$ (for <i>mc</i>)	−0.77	0.52	.143*	
$\hat{\beta}_5$ (for <i>m2</i>)	−4.53	0.67	.000	
$\hat{\beta}_6$ (for <i>m3</i>)	−7.39	0.67	.000	
$\hat{\beta}_7$ (for <i>m4</i>)	6.44	0.67	.000	
$\hat{\beta}_8$ (for <i>m5</i>)	10.67	0.67	.000	
$\hat{\beta}_0$ (constant)	23.92	1.11	.000	
LVEF				
$\hat{\beta}_1$ (for <i>filter</i>)	0.072	0.011	.000	0.8605
$\hat{\beta}_2$ (for <i>prone</i>)	−0.018	0.004	.000	
$\hat{\beta}_3$ (for <i>mr</i>)	−0.004	0.005	.385*	
$\hat{\beta}_4$ (for <i>mc</i>)	0.012	0.005	.017	
$\hat{\beta}_5$ (for <i>m2</i>)	−0.028	0.006	.000	
$\hat{\beta}_6$ (for <i>m3</i>)	0.053	0.006	.000	
$\hat{\beta}_7$ (for <i>m4</i>)	−0.057	0.006	.000	
$\hat{\beta}_8$ (for <i>m5</i>)	−0.131	0.006	.000	
$\hat{\beta}_0$ (constant)	0.564	0.010	.000	

Adapted from Boyd HL et al.¹

EDV = end-diastolic volume; ESV = end-systolic volume; LVEF = left ventricular ejection fraction; OLS = ordinary least squares.

*Insignificant ($p > .05$).

ECG-gated myocardial perfusion SPECT in mice. Qualitatively, the line profiles through the images and cardiac parameters that were derived from the images that were formed using three different motion correction strategies showed no large differences. Furthermore, we can discuss the influence of respiratory motion correction, image filtering, and animal positioning on the measured cardiac parameters by using our statistical model.

Influence of Strategies to Correct for Respiratory Motion

Only the motion-corrected strategy induced a statistically significant change to LVEF. However, the absolute change was 0.012, which is only 2.1% of the reference LVEF. Therefore, we could state that the different motion correction strategies that were tested in this work have no large influence on the measured cardiac parameters. In

Table 4. Interpretation of Statistically Significant Coefficients

<i>Estimate</i>	<i>Interpretation</i>
For EDV:	
$\hat{\beta}_1 = -6.7$	When FWHM of the gaussian filter increases by 1 mm, EDV decreases by 6.7 μL , ceteris paribus
$\hat{\beta}_2 = 3.1$	When position changes from supine to prone, EDV increases by 3.1 μL , ceteris paribus
For ESV:	
$\hat{\beta}_1 = -6.1$	When FWHM of the gaussian filter increases by 1 mm, ESV decreases by 6.1 μL , ceteris paribus
$\hat{\beta}_2 = 2.5$	When position changes from supine to prone, ESV increases by 2.5 μL , ceteris paribus
For LVEF:	
$\hat{\beta}_1 = 0.072$	When FWHM of the gaussian filter increases by 1 mm, LVEF increases by 0.072, ceteris paribus
$\hat{\beta}_2 = -0.018$	When position changes from supine to prone, LVEF decreases by 0.018, ceteris paribus
$\hat{\beta}_4 = 0.012$	When strategy changes from standard to motion corrected, LVEF increases by 0.012, ceteris paribus

EDV = end-diastolic volume; ESV = end-systolic volume; FWHM = full width half maximum; LVEF = left ventricular ejection fraction.

other words, compared to the “standard strategy,” neither the “motion-reduced strategy” nor the “motion-corrected strategy” induced changes in the cardiac parameters larger than 2.1%. Nevertheless, the “standard strategy” (i.e., ECG gating and no respiratory motion compensation) is the simplest strategy because it does not require recording and processing of respiratory signals.

Influence of Image Filtering

According to the estimated regression models, 5% changes relative to the reference EDV, ESV, and LVEF could be induced by, respectively, 0.37 mm, 0.18 mm, and 0.40 mm changes in the FWHM of the gaussian filter, with other factors remaining the same. In practice, researchers usually use the same filter for images from the same data set but may unconsciously use different filters for, for example, images reconstructed on different days in a longitudinal study before comparing them. One should be aware of this issue because, for example, once the difference of the FWHM of the filter exceeds 0.4 mm, there could be more than 5% errors in comparisons between the measured LVEFs.

Influence of Animal Positioning

An absolute change of about 3.1 μL (EDV), 2.5 μL (ESV), and 0.018 (LVEF) occurred when the animal positioning was changed, with other factors remaining the same. These are 6.2%, 11%, and 3.2% of the reference EDV, ESV, and LVEF, respectively. Although further experiments and analysis are needed to investigate the underlying reasons causing the observed changes, it is wise for

the same group of cardiac studies to keep the animal position the same.

The mouse model that was used in this study may play an important role as a preclinical model for evaluating the effects of therapeutics on cardiac function in future studies. In the current study, $^{99\text{m}}\text{Tc}$ -tetrofosmin was used. This tracer enables the quantification of myocardial perfusion and function in a single scan. In this study, we determined the influence of respiratory motion, image filtering, and animal positioning on cardiac parameters. There are still other effects, such as scatter and attenuation, that may influence the measurements, although these effects are very small and can be easily corrected in small animal imaging when clinical tracers are used.^{32–36}

In short, even for sub-half-millimeter myocardial SPECT, our results indicate that respiratory gating has no significant effect on measured cardiac parameters, whereas image filtering and the position of the animal(s) should be kept the same for all scans in a comparative study. Of course, it could be that when animals that are scanned under different anesthetic regimens or have compromised pulmonary function, quite different ranges of respiratory motion may occur. In such cases, simultaneous ECG and respiratory gating combined with respiratory motion correction may still be important and useful. Further investigations are required to study the possible effects on measured cardiac parameters under such conditions.

Conclusions

For high-resolution cardiac perfusion SPECT in mice, respiratory gating has no significant influence on measured

LTVs and LVEFs. Image filtering and animal positioning do have a large influence on these parameters and should therefore be kept the same for all scans in a comparative study.

Acknowledgments

We are grateful to Ruud Ramakers (MILabs B.V.), Inge Wolterink, John Buijs, and Bart J. Vermolen (University Medical Center Utrecht) for technical assistance and Marlies C. Goorden and Jarno van Roosmalen (Delft University of Technology) for valuable suggestions and comments.

Financial disclosure of authors: This research was partly performed within the framework of the Center for Translational Molecular Medicine, project EMINENCE (grant 01C-204). Chao Wu and Brendan Vastenhouw are employees of MILabs B.V. Freek J. Beekman is a stockholder of and gets honoraria and grant/research support from MILabs B.V. The other authors declare that they have no conflict of interest.

Financial disclosure of reviewers: None reported.

References

1. Boyd HL, Gunn RN, Marinho NV, et al. Non-invasive measurement of left ventricular volumes and function by gated positron emission tomography. *Eur J Nucl Med* 1996;23:1594–602.
2. Rajappan K, Livieratos L, Camici PG, et al. Measurement of ventricular volumes and function: a comparison of gated PET and cardiovascular magnetic resonance. *J Nucl Med* 2002;43:806–10.
3. Slart RH, Bax JJ, de Jong RM, et al. Comparison of gated PET with MRI for evaluation of left ventricular function in patients with coronary artery disease. *J Nucl Med* 2004;45:176–82.
4. Slart RH, Bax JJ, van Veldhuisen DJ, et al. Imaging techniques in nuclear cardiology for the assessment of myocardial viability. *Int J Cardiovasc Imaging* 2006;22:63–80, doi:[10.1007/s10554-005-7514-8](https://doi.org/10.1007/s10554-005-7514-8).
5. Boucher L, Rodrigue S, Lecomte R, et al. Respiratory gating for 3-dimensional PET of the thorax: feasibility and initial results. *J Nucl Med* 2004;45:214–9.
6. Lamare F, Ledesma Carbayo MJ, Cresson T, et al. List-mode-based reconstruction for respiratory motion correction in PET using non-rigid body transformations. *Phys Med Biol* 2007;52:5187–204, doi:[10.1088/0031-9155/52/17/006](https://doi.org/10.1088/0031-9155/52/17/006).
7. Klein GJ, Reutter BW, Ho MH, et al. Real-time system for respiratory-cardiac gating in positron tomography. *IEEE Trans Nucl Sci* 1998;45:2139–43, doi:[10.1109/23.708323](https://doi.org/10.1109/23.708323).
8. Livieratos L, Rajappan K, Stegger L, et al. Respiratory gating of cardiac PET data in list-mode acquisition. *Eur J Nucl Med Mol Imaging* 2006;33:584–8, doi:[10.1007/s00259-005-0031-0](https://doi.org/10.1007/s00259-005-0031-0).
9. Martinez-Moller A, Zikic D, Botnar RM, et al. Dual cardiac-respiratory gated PET: implementation and results from a feasibility study. *Eur J Nucl Med Mol Imaging* 2007;34:1447–54, doi:[10.1007/s00259-007-0374-9](https://doi.org/10.1007/s00259-007-0374-9).
10. Buther F, Dawood M, Stegger L, et al. List mode-driven cardiac and respiratory gating in PET. *J Nucl Med* 2009;50:674–81.
11. Gigengack F, Ruthotto L, Burger M, et al. Motion correction in dual gated cardiac PET using mass-preserving image registration. *IEEE Trans Med Imaging* 2012;31:698–712, doi:[10.1109/TMI.2011.2175402](https://doi.org/10.1109/TMI.2011.2175402).
12. Constantinesco A, Choquet P, Monassier L, et al. Assessment of left ventricular perfusion, volumes, and motion in mice using pinhole gated SPECT. *J Nucl Med* 2005;46:1005–11.
13. Vanhove C, Lahoutte T, Defrise M, et al. Reproducibility of left ventricular volume and ejection fraction measurements in rat using pinhole gated SPECT. *Eur J Nucl Med Mol Imaging* 2005;32:211–20, doi:[10.1007/s00259-004-1649-z](https://doi.org/10.1007/s00259-004-1649-z).
14. Goetz C, Monassier L, Choquet P, et al. Assessment of right and left ventricular function in healthy mice by blood-pool pinhole gated SPECT. *C R Biol* 2008;331:637–47.
15. de Kemp RA, Epstein FH, Catana C, et al. Small-animal molecular imaging methods. *J Nucl Med* 2010;51:18S–32S.
16. Golestani R, Wu C, Tio RA, et al. Small-animal SPECT and SPECT/CT: application in cardiovascular research. *Eur J Nucl Med Mol Imaging* 2010;37:1766–77, doi:[10.1007/s00259-009-1321-8](https://doi.org/10.1007/s00259-009-1321-8).
17. Strydom JH, Leenen FH, Ruddy TD, et al. Reproducibility of serial left ventricle perfusion, volume, and ejection fraction measurements using multiplexed multipinhole SPECT in healthy rats and rats after myocardial infarction. *J Nucl Med* 2011;52:1285–92.
18. Goethals LR, De Geeter F, Vanhove C, et al. Improved quantification in pinhole gated myocardial perfusion SPECT using micro-CT and ultrasound information. *Contrast Media Mol Imaging* 2012;7:167–74, doi:[10.1002/cmmi.477](https://doi.org/10.1002/cmmi.477).
19. Yang YF, Rendig S, Siegel S, et al. Cardiac PET imaging in mice with simultaneous cardiac and respiratory gating. *Phys Med Biol* 2005;50:2979–89, doi:[10.1088/0031-9155/50/13/001](https://doi.org/10.1088/0031-9155/50/13/001).
20. Vera P, Manrique A, Pontvianne V, et al. Thallium-gated SPECT in patients with major myocardial infarction: effect of filtering and zooming in comparison with equilibrium radionuclide imaging and left ventriculography. *J Nucl Med* 1999;40:513–21.
21. Wright GA, McDade M, Martin W, et al. Quantitative gated SPECT: the effect of reconstruction filter on calculated left ventricular ejection fractions and volumes. *Phys Med Biol* 2002;47:N99–105, doi:[10.1088/0031-9155/47/8/402](https://doi.org/10.1088/0031-9155/47/8/402).
22. Pai M, Yang YJ, Im KC, et al. Factors affecting accuracy of ventricular volume and ejection fraction measured by gated Tl-201 myocardial perfusion single photon emission computed tomography. *Int J Cardiovasc Imaging* 2006;22:671–81, doi:[10.1007/s10554-006-9098-3](https://doi.org/10.1007/s10554-006-9098-3).
23. Kakhki VRD, Sadeghi R. Gated myocardial perfusion SPECT in patients with a small heart: effect of zooming and filtering. *Clin Nucl Med* 2007;32:404–6, doi:[10.1097/01.rlu.0000259629.30918.88](https://doi.org/10.1097/01.rlu.0000259629.30918.88).
24. Lavender FM, Meades RT, Al-Nahhas A, et al. Factors affecting the measurement of left ventricular ejection fraction in myocardial perfusion imaging. *Nucl Med Commun* 2009;30:350–5, doi:[10.1097/MNM.0b013e328329d9ab](https://doi.org/10.1097/MNM.0b013e328329d9ab).
25. Berman D, Germano G, Lewin H, et al. Comparison of post-stress ejection fraction and relative left ventricular volumes by automatic analysis of gated myocardial perfusion single-photon emission computed tomography acquired in the supine and prone positions. *J Nucl Cardiol* 1998;5:40–7.
26. Schaefer WM, Lipke CS, Kuhl HP, et al. Prone versus supine patient positioning during gated ^{99m}Tc-sestamibi SPECT: effect on

- left ventricular volumes, ejection fraction, and heart rate. *J Nucl Med* 2004;45:2016–20.
27. Yap K, Campbell P, Cherk M, et al. Effect of prone versus supine positioning on left ventricular ejection fraction (LVEF) and heart rate using ECG gated Tl-201 myocardial perfusion scans and gated cardiac blood pool scans. *J Med Imaging Radiat Oncol* 2012;56:525–31, doi:[10.1111/j.1754-9485.2012.02438.x](https://doi.org/10.1111/j.1754-9485.2012.02438.x).
 28. van der Have F, Vastenhouw B, Ramakers RM, et al. U-SPECT-II: an ultra-high-resolution device for molecular small-animal imaging. *J Nucl Med* 2009;50:599–605.
 29. Branderhorst W, Vastenhouw B, Beekman FJ. Pixel-based subsets for rapid multi-pinhole SPECT reconstruction. *Phys Med Biol* 2010;55:2023–34, doi:[10.1088/0031-9155/55/7/015](https://doi.org/10.1088/0031-9155/55/7/015).
 30. Klein S, Staring M, Murphy K, et al. elastix: a toolbox for intensity-based medical image registration. *IEEE Trans Med Imaging* 2010;29:196–205, doi:[10.1109/TMI.2009.2035616](https://doi.org/10.1109/TMI.2009.2035616).
 31. Ficaro EP, Lee BC, Kritzman JN, et al. Corridor4DM: the Michigan method for quantitative nuclear cardiology. *J Nucl Cardiol* 2007;14:455–65.
 32. Chen CL, Wang Y, Lee JJ, et al. Toward quantitative small animal pinhole SPECT: assessment of quantitation accuracy prior to image compensations. *Mol Imaging Biol* 2009;11:195–203, doi:[10.1007/s11307-008-0181-0](https://doi.org/10.1007/s11307-008-0181-0).
 33. Vanhove C, Defrise M, Bossuyt A, et al. Improved quantification in single-pinhole and multiple-pinhole SPECT using micro-CT information. *Eur J Nucl Med Mol Imaging* 2009;36:1049–63, doi:[10.1007/s00259-009-1062-8](https://doi.org/10.1007/s00259-009-1062-8).
 34. Wu C, van der Have F, Vastenhouw B, et al. Absolute quantitative total-body small-animal SPECT with focusing pinholes. *Eur J Nucl Med Mol Imaging* 2010;37:2127–35, doi:[10.1007/s00259-010-1519-9](https://doi.org/10.1007/s00259-010-1519-9).
 35. Wu C, de Jong JR, Gratama van Andel HA, et al. Quantitative multi-pinhole small-animal SPECT: uniform versus non-uniform Chang attenuation correction. *Phys Med Biol* 2011;56:N183–93, doi:[10.1088/0031-9155/56/18/N01](https://doi.org/10.1088/0031-9155/56/18/N01).
 36. Wu C, Gratama van Andel HA, Laverman P, et al. Effects of attenuation map accuracy on attenuation-corrected micro-SPECT images. *EJNMMI Res* 2013;3:7, doi:[10.1186/2191-219X-3-7](https://doi.org/10.1186/2191-219X-3-7).